

Energy transport along FPU- β chains containing binary isotopic disorder: Zero temperature systems

K.A. Snyder

Materials and Construction Division, National Institute of Standards and Technology

T.R. Kirkpatrick

Institute for Physical Science and Technology and Department of Physics, University of Maryland

(Dated: September 27, 2018)

Dissipation from harmonic energy eigenstates is used to characterize energy transport in binary isotopically disordered (BID) Fermi-Pasta-Ulam (FPU- β) chains. Using a continuum analog for the corresponding harmonic portion of the Hamiltonian, the time-independent wave amplitude is calculated for a plane wave having wavelength λ that is incident upon the disordered section, and the solution is mapped onto the discrete chain. Due to Anderson localization, energy is initially localized near the incident end of the chain, and in the absence of anharmonicity the wave amplitude is stationary in time. For sufficient anharmonicity, however, mode transitions lead to dissipation. Energy transport along the chain is quantified using both the second moment M of the site energy, and the number of masses contributing to transport, which was estimated from the localization parameter. Over the time scales studied, M increased linearly in time, yielding an effective transport coefficient G . At low and intermediate impurity concentration c , $G(c)$ can be characterized by a competition between the rate of mode transitions and the time for energy to propagate a distance equal to the localization length ξ . At the highest concentrations ($1.6 \leq c\lambda \leq 16.0$), there is significant mode transition suppression in BID systems, and the transport coefficient $G(c)$ becomes proportional to $\xi(c)$.

PACS numbers: 45.05.+x, 45.30.+s, 46.40.Cd, 62.20.Pw,

I. INTRODUCTION

Nonlinear binary disordered chains are a useful systems for studying the essential characteristics of energy dissipation and transport in materials. Although binary disorder is an idealized model, it has practical application to a number of fields: isotopic disorder effects line width broadening in spectroscopy;^{1,2,3} the glass transition has been considered in terms of binary changes in elasticity parameters;⁴ and isolated mechanical defects that occur in practice can lead to a variety of nonlinear effects.^{5,6}

An interesting behavior of binary isotopic disorder (BID) occurs in discrete lattices, where the system undergoes a pure-disordered-pure transition as the impurity concentration varies from zero to one. For harmonic one-dimensional chains composed of discrete elements, finite disorder destroys spatial invariance and gives rise to Anderson⁷ localization, characterized by spatially localized eigenstates. Given a discrete system in a localized energy eigenstate, the addition of anharmonicity will lead to interactions that create new modes that can propagate through the system. These propagating modes either will become localized or will undergo further mode transitions.

We are interested in the rate of energy dissipation from localized disturbances. Previous studies of dissipation have used either a singular (one or very few elements) pulse or a Gaussian pulse for the initial displacement.^{8,9,10,11,12} Because neither is an eigenstate of the system, the singular pulse will spread and the Gaussian pulse will propagate ballistically in both

anharmonic and harmonic systems. For Gaussian and ‘kicked’ singular pulses, the initial behavior is ballistic. In time, scattering and localization slow the rates of propagation and dispersion.

To eliminate the initial ballistic motion, the system can be started in an energy eigenstate of the corresponding harmonic chain. The middle section of the chain contains disorder, and there are “pure” sections at both ends. Given the location of each impurity in the disordered section of the chain, a solution is found for the continuum analog, with the boundary condition of an incident plane wave with frequency ω ; there is a reflective wave and a transmitted wave. Because the continuum calculation is performed for the harmonic system, the solution is separable into spatial and temporal components. The time dependence is sinusoidal, and the entire system has a constant temporal phase. The continuum solution for the wave amplitude everywhere is mapped onto the discrete chain, and becomes the initial displacement.

The advantage of this approach is that in the absence of anharmonicity the wave amplitude is stationary. For the harmonic chain, the wave remains localized indefinitely, and there is no energy transport. The addition of anharmonicity will give rise to mode transitions that will de-localize the wave and lead to energy transport through the chain. Instead of having a ballistic-diffusive transition, this initial condition leads to a localized-diffusive transition.

The remaining question is whether the energy will dissipate in a diffusive manner. In one-dimensional systems, mode interactions can lead to frequencies arbitrarily close

to zero. Because the localization length of these modes is proportional to ω^{-2} and the scattering cross section is proportional to ω^2 , these low frequency modes should propagate ballistically in a finite system. Because the energy content of these modes is proportional to ω^2 , however, it is unlikely that these ballistic modes contribute substantially to energy transport.

To study this energy transport, the following numerical experiment will use the binary disordered Fermi-Pasta-Ulam¹³ chain with quartic spring potentials (FPU- β). Starting from the initial energy eigenstate, numerical integration will be used to calculate the spatial distribution of energy as a function of time. Based on a local concept of thermal transport,⁴ an effective transport coefficient will be sought from the second moment of the site energy, and the method is compared to the Helfand¹⁴ moments for thermal conductivity. The second moment will exhibit diffusive behavior, a fact that will be corroborated qualitatively from the number of masses that energy is distributed, which is estimated from the localization parameter.^{15,16}

II. NUMERICAL EXPERIMENT

A. FPU- β Chain

The FPU- β chain is composed of masses interacting with nearest neighbors through springs. The Hamiltonian H of a chain having N masses is function of the mass momenta p_i and the mass displacements q_i about their equilibrium position:

$$H = \sum_i \frac{p_i^2}{2m_i} + \frac{K}{2}(q_i - q_{i-1})^2 + \frac{\beta}{4}(q_i - q_{i-1})^4 \quad (1)$$

The harmonic spring force coefficient K is set equal to one, and in the absence of impurities, each mass has the same value $m_o=1$. The site energy E_i is the sum of the kinetic energy plus one-half of the neighboring spring potential energies. The total energy E_T is the sum of the site energies.

Whenever possible, the results are expressed in dimensionless units through the use of appropriate scaling factors. Time is scaled by the natural frequency ω_o of a single harmonic oscillator:

$$\omega_o = \left(\frac{K}{m_o} \right)^{1/2} \quad (2)$$

Lengths are scaled by the equilibrium mass separation distance a .

The time-dependent behavior was determined by numerical integration using the sixth-order Yoshida¹⁷ symplectic integration algorithm. Specifically, best results were obtained from the ‘‘Solution A’’ coefficients (see Table 1 in Ref. 17). For the systems studied here, the time step Δt was approximately 1/200 the period of the initial mode. This time step was consistent with that used

elsewhere,^{8,18} was chosen as a compromise between speed and accuracy, and the results were insensitive to two-fold changes in Δt . Using this time step, the energy fluctuations were always less than 0.2 % (See Appendix).

B. Semi-Infinite Approximation

In most cases, low frequency waves will propagate down the chain and reach the far end. If the wave is reflected, it could affect the accuracy of the transport calculation. To mitigate this effect, 10 % of the masses at the far end were given a viscous force F_{vis} :

$$F_{vis} = -\eta \dot{q} \quad (3)$$

This approach has been used elsewhere to achieve a similar effect.¹⁹ For these calculations, a viscosity η of 0.2 was sufficient to eliminate the effects of reflection.

The viscous damping, combined with the accurate time integration, simplified the task of identifying finite size effects. As the system length decreased and the localization length increased, the likelihood of a considerable amount of energy reaching the far end of the system increased. Fortunately, this occurrence was easily identified by changes in the system total energy.

C. Initial Displacement

The initial condition was a stationary state exhibiting Anderson localization for the harmonic component of the Hamiltonian. This initial condition was chosen so that for $\beta=0$ there is no net energy transport, and these systems could be used as a test to confirm the accuracy of the model and the numerical integration.

The continuum Kronig-Penney liquid model^{20,21} is used to estimate the initial displacement. For the harmonic FPU chain, the analogous continuum system is an elastic rod having mass density $\mu = m_o/a$ and Youngs modulus $Y = Ka$. Between the impurities, a longitudinal wave $\psi(x, t|\omega)$ with frequency ω will propagate with velocity $c_l = \sqrt{Y/\mu}$. A harmonic oscillator impurity, approximated by a point defect, located at x' will give rise to a reactive force due to the impurity impedance Z to a wave with frequency ω :²²

$$\left[\mu \frac{\partial^2}{\partial t^2} - Y \frac{\partial^2}{\partial x^2} = -Z(\omega) \delta(x - x') \frac{\partial}{\partial t} \right] \psi(x, t|\omega) \quad (4)$$

For a harmonic system such as this, one can assume a sinusoidal solution with frequency ω ($\psi = \phi(x|\omega) e^{-i\omega t}$):

$$\left[\frac{\partial^2}{\partial x^2} + \zeta^2 = \frac{-i\omega}{Y} Z(\omega) \delta(x - x') \right] \phi(x|\omega) \quad (5)$$

where $\zeta = \omega/c_l$.

Equation (5) is solved for a system having impurities at integer locations with probability c . The boundary conditions are a unit amplitude incident wave and a reflected wave at one end and only a transmitted wave at the other end. The initial displacement for the physical system of masses and springs is taken from the real component of the solution $\phi(x|\omega)$.

D. Impurity Cross Section

To put some of the results in a familiar context, it will be useful to characterize an impurity by its cross section to the original wave. The cross section σ of an individual impurity can be expressed as a function of the impurity impedance Z :²²

$$\sigma = \frac{|Z(\omega)|^2}{|Z(\omega)|^2 + 4Km_o} \quad (6)$$

The isotopic impurities consist of a constant mass m_+ added to the existing mass m_o ; m_+ may be either positive or negative. (The impurity mass $m_I = m_o + m_+$.) The impedance Z of a mass impurity in a continuum system²² is modified by c_s , which is the ratio of the group velocity ($v_g = \partial\omega/\partial k$) to the longitudinal velocity c_l :²³

$$Z(\omega) = -i\omega m_+/c_s \quad (7)$$

For the discrete chain, $c_s = \cos(ka/2)$, where k is the wavenumber ($2\pi/\lambda$) and λ is the displacement wavelength.

E. Continuum-Discrete Mapping

The boundary condition for the chain is zero displacement at each end. Because the continuum solution $\phi(x=0, L|\omega)$ will (with almost certainty) not equal zero at $(x=0, L)$, a method is needed for adjusting the continuum solution to accommodate the constraints of the discrete chain. The continuum solution is first mapped to the discrete chain with no modification, and then, starting at the end and searching along the chain, the end is relocated at the mass having the smallest oscillation amplitude. The end is relocated to this mass, and its displacement is fixed at zero. The process is repeated at the opposite end of the chain.

To facilitate this task, a suitable initial displacement wavelength λ is needed to ensure that some mass has an equilibrium displacement acceptably close to zero. If the displacement wavelength is an integer multiple of the equilibrium mass displacement a , the oscillation amplitude of masses along each successive wavelength remains constant, until the next impurity changes the phase.

For this experiment, a nominal displacement (equal to an integer multiple of the unit spacing) is chosen first.

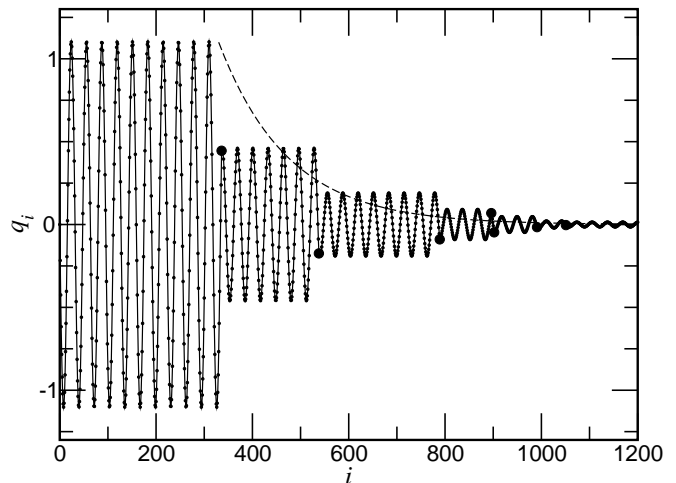


FIG. 1: Initial displacements q_i for a particular system having wavelength 31.8, impurity concentration 0.01, and impurity scattering cross section 0.5. Mass displacement are denoted by small circles and the impurity locations are denoted by large circles. The first impurity is located at $i = \iota$, and the dashed line is proportional to $e^{-(i-\iota)/\xi}$.

The working wavelength is the nominal wavelength minus 0.2 unit spacings. With this wavelength, the displacement closest to zero repeats every 5 wavelengths, with 9 nodal points occurring at different fractions of the spacing a . Probabilistically, this reduces the minimum mass oscillation amplitude by nearly an order of magnitude over an integer wavelength.

An example input displacement is shown in Fig. 1 for a system with length 10 000, displacement wavelength 31.8, impurity cross section 0.5, and impurity concentration 0.01. The small dots in the figure represent the displacement of the masses. The larger filled circles denote the location of impurities. The effect of the impurities is to change both the the displacement amplitude and phase. Also shown in the figure is a dashed line that is proportional to $e^{-(i-\iota)/\xi}$, where ι is the location of the first impurity. Although this particular initial condition would suggest that the displacement amplitudes decrease monotonically, that is not always the case.

F. Dense Systems

For BID systems, the localization length is not a monotonic function of impurity concentration. Rather, the localization length has a minimum with respect to impurity concentration; at higher concentrations, the system returns to a “pure” system. The localization length ξ of BID systems at dilute impurity concentrations, such that $c\lambda \ll 1$, can be calculated from the resistivity scaling law:²⁵

$$\xi_{c \rightarrow 0}^{-1} = c \ln(1 + \rho) \quad (8)$$

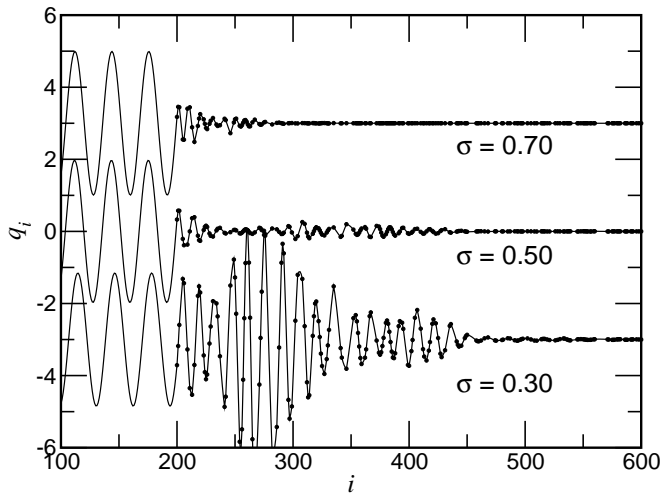


FIG. 2: Initial displacements q_i for a particular system having wavelength 31.8, impurity concentration 0.50, and all three impurity scattering cross sections. Mass displacement are denoted by line, and the impurity locations are denoted by circles. The systems were shifted horizontally so that the first impurity is located at $i = 200$.

The single impurity resistivity ρ is related to the single impurity cross section σ :²⁶

$$\rho = \frac{\sigma}{1 - \sigma} \quad (9)$$

As the impurity concentration increases, the system approaches a homogeneous system. In the limit $c \rightarrow 1$, the system is again ordered, and the localization length diverges:

$$\xi_{c \rightarrow 1}^{-1} = (1 - c) \ln(1 + \rho') \quad (10)$$

The quantity ρ' characterizes a system having an equilibrium mass ($m_o + m_+$), an impurity mass m_o , and the system oscillates at the same frequency ω :²³

$$k' = \frac{2}{a} \text{Sin}^{-1} \left[\frac{\omega}{2} \sqrt{\frac{m_o + m_+}{K}} \right] \quad (11a)$$

$$c'_s = \cos(k'a/2) \quad (11b)$$

$$\rho' = \frac{(-m_+\omega/c'_s)^2}{4K(m_o + m_+)} \quad (11c)$$

The relation for k' in Eq. (11a) is an improvement over the low frequency approximation given previously.²³ Because the localization length is analogous to conductivity, and the systems described by $\xi_{c \rightarrow 0}$ and $\xi_{c \rightarrow 1}$ occur independently and in parallel, the localization length over all values of impurity concentration can be approximated by a sum of the two:²³

$$\xi = \xi_{c \rightarrow 0} + \xi_{c \rightarrow 1} \quad (12)$$

When the concentration of the impurities increases to $c\lambda > 1$, the energy eigenstate becomes more complicated

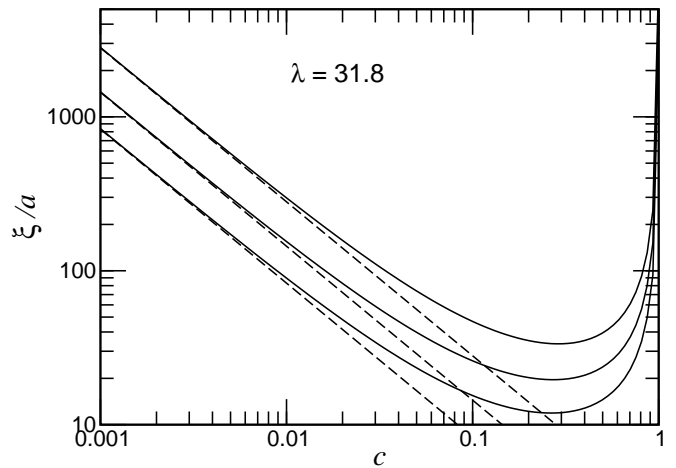


FIG. 3: Localization length ξ as a function of impurity concentration c for systems having displacement wavelength $\lambda = 31.8$. The three solid curves, from upper to lower, are for $\sigma = 0.30, 0.50$, and 0.70 . The dashed lines are the dilute limit localization length $\xi_{c \rightarrow 0}$.

than the dilute impurity example shown in Fig. 1. Example initial conditions for the highest impurity concentration considered in this experiment ($c = 0.5$) are shown in Fig. 2 for three scattering cross sections. At these high concentrations, although the frequency remains constant everywhere, the wave structure in the disordered region is complex.

G. Parameter Space

For the nonlinear systems considered, the incident wave has wavelength $\lambda = 31.8$, and the anharmonicity parameter $\beta = 1$. For all the systems from which energy transport is measured, the added mass m_+ will have one of three values: 6.605, 10.089, and 15.412. With respect to a $\lambda = 31.8$ displacement in a harmonic system, these impurity masses have scattering cross sections 0.30, 0.50, and 0.70, respectively.

The initial displacement is a localized mode with localization length ξ . The localization lengths calculated from Eq. (12) for $\lambda = 31.8$ and the three impurity masses mentioned are shown in Fig. 3 as a function of impurity concentration c . The dilute limit result $\xi_{c \rightarrow 0}$ is shown as a dashed line, and begins to depart from ξ near $c\lambda \sim 1$.

Figure 3 also reveals the utility of choosing a nominal displacement wavelength $\lambda = 32$. For $c\lambda > 1$, the addition of impurities has a nonlinear effect on localization length. Naturally, one would like to see whether this nonlinear behavior has any effect on energy transport. For shorter displacement wavelengths, the deviation between ξ and $\xi_{c \rightarrow 0}$ would not occur until proportionately higher impurity concentrations. Alternatively, using a longer wavelength would reduce the rate of mode transitions considerably, requiring excessively long computa-

tional times.

III. THERMAL CONDUCTION

There are a number of formal methods for calculating thermal conductivity. Thermostats at the boundaries can generate a steady-state flux from which the thermal conductivity is calculated using Fourier's law.²⁷ The Green-Kubo method²⁸ is based on time integrals of thermal fluxes for a system in thermal equilibrium. The Evans NEMD thermal conductivity algorithm^{28,29} applies a heat field and calculates an averaged heat flux. The Helfand¹⁴ moments of the excess energy fluctuations are calculated for systems in thermal equilibrium. In each case, the system is some state of steady-state or thermal equilibrium, which does not apply here.

Elsewhere, the second moment of the site energy has been used to characterize pulse dissipation.^{8,9,10,11,12} This approach bears a qualitative resemblance to the method of Helfand, which is based on mean squared fluctuations of excess energy. Here, a brief summary of the Helfand moments for thermal conductivity is used to motivate the relevance of the second moment of the site energy in nonequilibrium chains at zero temperature.

The thermal conductivity of a collection of freely moving particles in thermal equilibrium can be determined from energy fluctuations. The energy fluctuation \tilde{E}_i for the i -th particle is the difference between the instantaneous site energy E_i and the ensemble averaged value $\langle E_i \rangle$:

$$\tilde{E} = E_i - \langle E_i \rangle \quad (13)$$

If the energy fluctuation is conserved, and the energy flux has a linear dependence on $\nabla \tilde{E}$, the quantity $\tilde{E}_i(x, t)$ will satisfy the diffusion equation. For the boundary conditions that the initial value $\tilde{E}_i(x, 0)$ is localized about x_{i0} , and that $\tilde{E}_i(\pm\infty, t) = 0$, the solution for $\tilde{E}_i(x, t)$ is Gaussian, and the measure of spread is the second moment of \tilde{E}_i :

$$\int (x - x_{i0})^2 \tilde{E}(x, t) dx \sim 2\tilde{E}_i(x, 0)\kappa t \quad (14)$$

where κ is the thermal conductivity.

As \tilde{E}_i represents the fluctuation for a single particle, a bulk expression requires an ensemble integral of the second moment. Making no assumption about the independence of particle energies, the thermal conductivity can be calculated from a double sum over particle positions:¹⁴

$$H^p = \left\langle \sum_{i,j} (x_i - x_{j0})^2 \tilde{E}_i(x, t) \tilde{E}_j(x, 0) \right\rangle \sim 2\kappa t \quad (15)$$

Replacing conservation of momentum with conservation

of energy yields an equivalent alternative expression:¹⁴

$$H^e = \left\langle \left[\sum_i (x_i \tilde{E}_i - x_{i0} \tilde{E}_{i0}) \right]^2 \right\rangle \sim 2\kappa t \quad (16)$$

Equations (15) and (16) are the Helfand moments for calculating the thermal conductivity of a bath of particles.

There are a number of differences between fluctuations in a bath of particles and energy propagation along a discrete chain. Equations (15) and (16) characterize a bath of freely moving particles. By contrast, in the FPU chain, energy moves, but the masses are, more or less, stationary. This is not entirely problematic, however, because one can still evaluate the energy that is at x_i . The problem can be changed to one in which the energy is evaluated at specific points. In this way, the role of energy is analogous to concentration in the evaluation of self-diffusion.

Another important distinction is that Eqs. (15) and (16) are functions of the energy fluctuations in a system in equilibrium at temperature T . By contrast, the pulse moving through the FPU chain is a system that is not in equilibrium, and the portion of the chain farthest from the initial disturbance is initially at zero temperature. In principle, after very long times, the chain would eventually reach equilibrium, with the energy distributed over all the masses. Because the conceptual problem of interest is a semi-infinite chain, the equilibrium energy $\langle E_i \rangle$ would approach zero. Under this assumption, the fluctuation energy \tilde{E} of the bath problem becomes the site energy E_i of the non-equilibrium chain problem.

By analogy to Eqs. (15) and (16), the energy transport in the FPU- β chain will be characterized by the second moment of the energy. Assuming that the initial pulse occupies a small portion of the entire system, a useful measure is the second moment about zero:

$$\frac{\sum_i r_i^2 E_i}{\sum E_i} \sim 2Gt \quad (17)$$

The position $r_i = ia$ is the equilibrium location of the i -th mass. The quantity G is an effective transport coefficient that is neither self-diffusion nor thermal conductivity. To eliminate the effects of fluctuations, the initial value is subtracted from the subsequent values. In addition, the equation is generalized to allow for arbitrary powers of E_i :

$$M_n(t) = \left\langle \frac{\sum_i r_i^2 E_i^n}{\sum E_i^n} - M_n(0) \right\rangle \sim 2G_n t \quad (18)$$

These definitions are similar to those used by Frölich et al.,³⁰ and are consistent with the local concept of thermal transport of Wagner et al.⁴

A comparison among M_1 , M_2 , H^p , and H^e is made from the early response of a system of length 8000 that is initially in a localized mode. The wavelength is 31.8, the impurity mass is 11.089, the impurity concentration

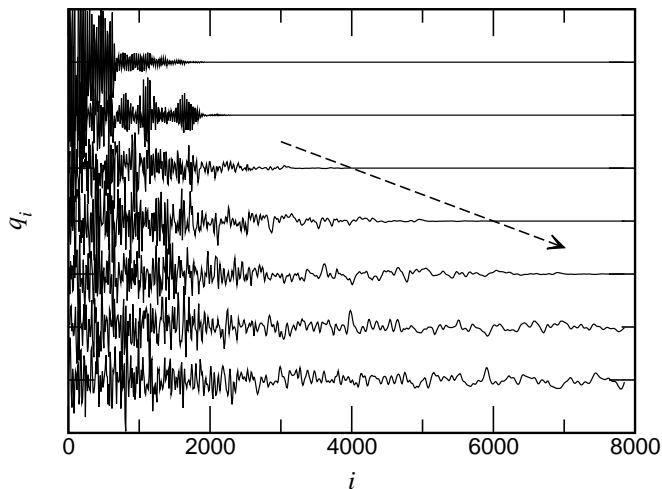


FIG. 4: Wave displacement q_i along a chain at various times. Chain length is 8000, added mass m_+ is 10.089, and impurity concentration is 0.010. Each curve represents a time difference of 2000, and is offset by a value of one for demonstration purposes. Dashed arrow denotes ballistic propagation.

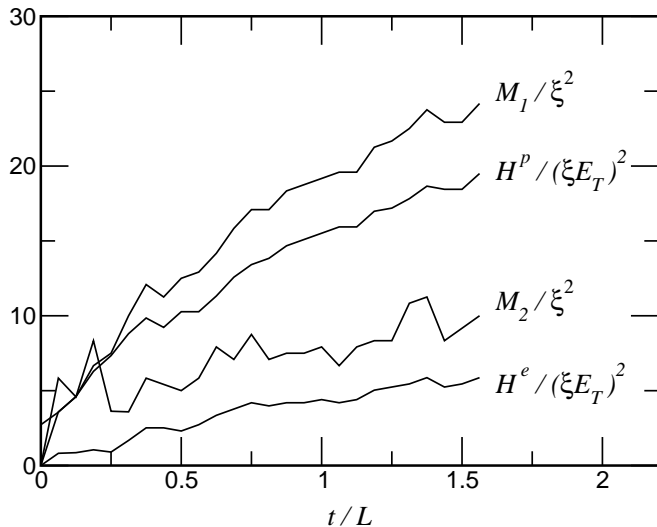


FIG. 5: Moments M_1 , M_2 , H^p , H^e as a function of time for the system shown in Fig. 4. Quantities are normalized, using localization length ξ and total energy E_T , to make the values dimensionless.

is 0.010, and $\beta = 1$. The displacement q along the system is shown in Fig. 4 at time intervals of $\Delta\omega_0 t = 2000$. (The curves are offset vertically from one another, by a distance a , for comparison purposes.) The data in the figure show that long wavelength displacements move virtually ballistically along the chain (parallel to dashed arrow) while the higher frequency displacements propagate a considerably shorter distance over the same time interval.

At regular time intervals, M_1 and M_2 are calculated, along with H^p and H^e (assuming that $\tilde{E} = E_i$ and $\langle E_i \rangle = 0$). The results of the calculations are shown

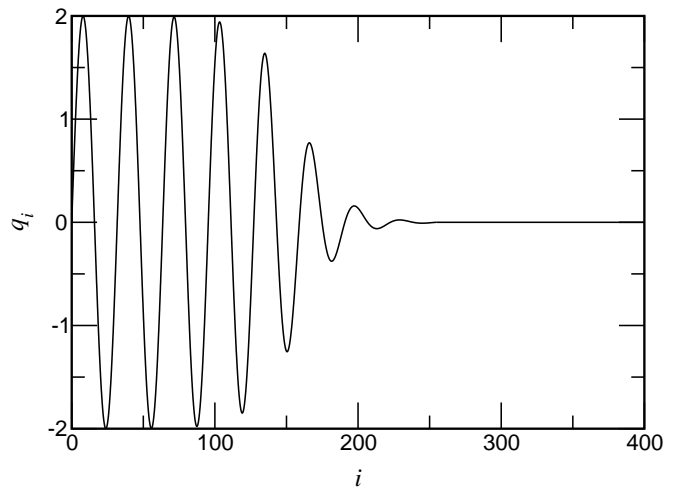


FIG. 6: Displacement q_i for sinusoid initial condition with $\lambda = 31.8$.

in Fig. 5. All values are normalized by the initial localization length ($\xi \approx 155$). H^p and H^e are also normalized by the total energy E_T to be on the same scale as M_1 and M_2 . The two pairs of equations correspond well to one another. Generally, M_1 and M_2 are greater in value than the corresponding H^p and H^e . At the shortest times, M_1 and H^p give the nearly the same value.

H^p and H^e are equivalent descriptions of thermal conductivity. Therefore, the difference between H^p and H^e for the case of an initially localized pulse demonstrates that thermal conductivity for these systems is not well-defined. As a result, the second moments M_n characterize some effective, yet undefined, transport coefficient.

These curves are also instructive in pointing out the distinction between pulse propagation and energy propagation. From Fig. 4 it is clear that low frequency waves propagate ballistically through these systems, starting from near $t = 0$. By contrast, Fig. 5 shows no ballistic behavior, suggesting that the vast majority of the energy is in the higher frequency modes located within the initially localized region. Moreover, the moments shown in Fig. 5 all continue to increase after there has been sufficient time for the low frequency ballistic modes to reach the far end.

IV. INITIAL CONDITION

The initial condition, composed of a localized mode, has the advantage of spatial stability. In the absence of anharmonicity, the initial wave will oscillate with a periodic amplitude that is constant in time.

Alternatively, this experiment could have been performed using either an instantaneous impulse or a short sinusoidal pulse like that shown in Fig. 6. Both of these initial conditions, however, have drawbacks. Impulses will impart relatively little energy to the system unless the impulse is large. The sinusoidal wave, not being lo-

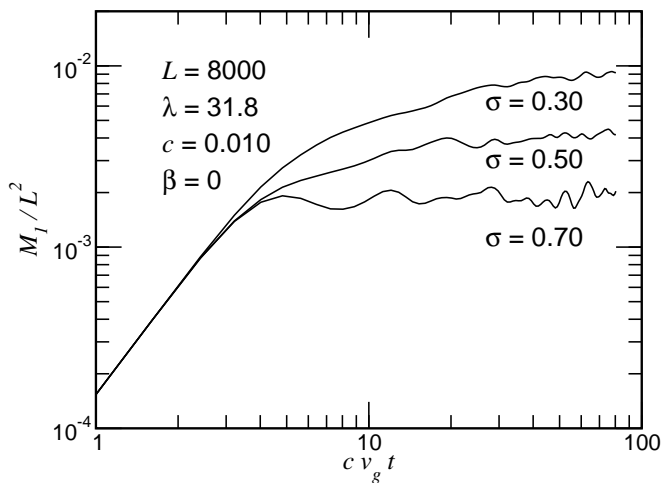


FIG. 7: M_1 as a function of time t for systems with anharmonic parameter $\beta = 0$ and impurity concentration $c = 0.010$ for systems having length $L = 8000$.

calized by the impurities, will immediately begin propagating ballistically along the chain. If the chain had only harmonic interactions, the wave would eventually settle into a localized state. In a nonlinear chain there will be immediate competition between localization of the initial wavelength and anharmonic effects that would lead to mode transitions that would then experience the same competition.

The time required for the sinusoidal pulse to become localized in a harmonic chain is shown in Fig. 7 for the $\lambda = 31.8$ pulse shown in Fig. 6. The pulse is located at one end of the system, the envelope is the hyperbolic tangent function, and the initial velocity is zero. The harmonic chains have mass impurities located at a site with probability c . Three different different values for m_I are considered, corresponding to $\sigma = 0.30, 0.50$, and 0.70 . The data in Fig. 7 suggest that somewhere between 10 and 100 impurities, depending on the impurity cross section, must be encountered before the sinusoidal wave becomes localized. The localization length for these three cross sections are 298, 155, and 90, respectively, so the transient period is approximately ten times the localization length. For the lowest impurity concentrations considered in this experiment, this transition length would have made the required system length prohibitively long.

V. EQUIPARTITION

The rate of both mode transitions and spatial energy equipartition will influence the response of the systems. The mode transition rate for similar chains configured as small hoops initially excited in a single eigenmode studied previously³¹ suggests that impurities initially hasten the decay of energy in the excited mode. Over long times, however, the rate diminished because the energy became localized at the impurities. Because the impurities were

heavier than the background, the oscillations at the impurities was smaller, reducing the rate of energy loss because of the quadratic dependence of amplitude.

The systems studied here, however, have energy initially localized at one end, with the energy already localized at the impurities. Once transitions start to occur, the new modes, which are not localized over the same length scale, will propagate and both spontaneously decay and collide with impurities.

A. Localization Parameter

As the mode transitions occur, energy will propagate along the chain, redistributing energy. As the energy becomes more evenly distributed among the masses, the energy becomes less localized. A measure of how uniformly the energy is distributed among N masses is the localization parameter Γ :^{15,16}

$$\Gamma = N \left\langle \frac{\sum^N E_i^2}{\left(\sum^N E_i\right)^2} \right\rangle \quad (19)$$

The value of Γ is a minimum for ergodic behavior and increases as the degree of localization increases.

The localization parameter can be used to estimate the number of masses over which energy is distributed. The maximum value of Γ is N , when all the energy is localized at one mass. At long time, Γ approaches a constant, $\Gamma_\infty = \Gamma(t \rightarrow \infty)$, that only depends on the value of β .³² For the FPU- β system, with $\beta = 1$, the equilibrium value Γ_∞ is approximately 1.8. Thus, Γ_∞/Γ is approximately equal to the portion of the chain over which energy is distributed.

B. Participating Modes

Another useful measure of ergodicity is the number of harmonic modes contributing to the overall energy at a mass. The systems studied will be initially excited in one mode (in frequency space). The time required for the system to excite the maximum number of modes should correspond to the time required for the system to become ergodic.

The energy in a particular mode E_ω is estimated from the harmonic approximation involving the Fourier transformed (FT) displacement $Q_i(\omega)$ and momentum $P_i(\omega)$ of mass m_i :

$$E_{i,\omega} = \frac{1}{2} \left(m_i \omega^2 Q_i^2 + \frac{P_i^2}{m_i} \right) \quad (20)$$

The energy is then normalized using the total number of frequency modes N_ω considered in the FT:

$$e_{i,\omega} = E_{i,\omega} / \sum_\omega^{N_\omega} E_{i,\omega} \quad (21)$$

These normalized energies are a measure of energy entropy S_i at mass m_i :^{15,18,33,34}

$$S_i = - \sum_{\omega} e_{i,\omega} \ln(e_{i,\omega}) \quad (22)$$

If all the energy is in a single frequency mode, S equals 0. If the energy is distributed evenly among all frequency modes, $S = \ln N_{\omega}$.

The alternative expression for the energy entropy is $\exp(S)$. This quantity is the equivalent number of modes contributing to the overall entropy if the energy is uniformly distributed among those modes. To make comparisons among results using different values for N_{ω} , results are expressed as the fraction of modes n_{ω} :

$$n_{\omega}^{(i)} = \frac{\exp(S_i)}{N_{\omega}} \quad (23)$$

Periodically, $n_{\omega}^{(i)}$ is calculated at various masses and the reported value, $n_{\omega}(t)$, is the average of these values.

C. Hoop Example

The localization parameter Γ and the fraction of participating modes n_{ω} were developed to study systems in which the energy is initially distributed throughout. For the systems studied here, the initial energy is intentionally localized at one end of the system. If such a system was divided into two equal halves, the values for Γ and n_{ω} in one half would be very different from the ones calculated for the other half of the system. Nonetheless, the parameters do have utility for these systems.

One application is the study of behavior within a short section of chain. If the section of chain is quasi-localized (very few modes are present, oscillating with nearly constant amplitude), mode transitions are the primary mechanism for inducing energy transport. A hoop (periodic boundary conditions), initially excited in one wave number mode, could be used to study the behavior of a similar section within a much longer section that is itself quasi-localized. The time-dependent behavior of the localization parameter Γ and the relative number of participating modes n_{ω} would characterize energy redistribution, with respect to both space and mode frequency.

A brief numerical calculation of Γ and n_{ω} is made to study the effect. The initial condition is a BID hoop having length 318, wavelength 31.8, and $\beta = 1$. This initial condition differs from a localized state. In a disordered system, a single k mode will excite multiple ω modes, accelerating the initial rate of mode transitions. Nevertheless, the results illuminate general behavior for nonlinear BID systems.

The effects of impurity concentration on energy distribution and on mode production are shown in Figs. 8 and 9. For dilute systems ($c\lambda < 1$), the time required for energy to be distributed among all the masses is nearly a

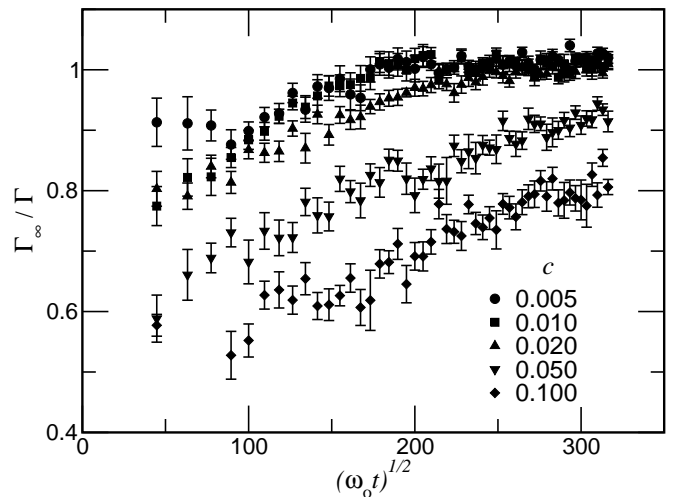


FIG. 8: Localization parameter Γ as a function of time t for a periodic system with length 636, initial wavelength 31.8, impurity cross section 0.5, and anharmonicity 1.0.

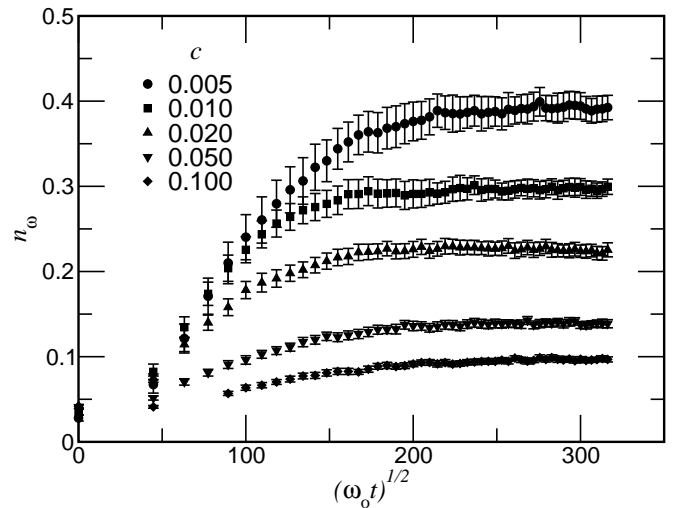


FIG. 9: Fraction of participating modes n_{ω} as a function of time t for a periodic system with length 636, initial wavelength 31.8, impurity cross section 0.5, and anharmonicity 1.0.

constant. For concentrated systems ($c\lambda > 1$), the spatial redistribution of energy is slowed dramatically.

This behavior is consistent with the data for n_{ω} in Fig. 9. The rate that new modes are produced in dilute systems is a constant, until n_{ω} approaches its asymptotic value. At concentrations for which $c\lambda > 1$, however, the initial rate of mode production does not reach the common initial rate. The asymptotic value for n_{ω} decreases with increasing impurity concentration. Therefore, concentrated systems produce fewer modes at a slower rate than less concentrated systems.

The decreasing asymptotic value for n_{ω} with increasing impurity concentration indicates that modes are suppressed significantly in concentrated systems. This is consistent with the effect of impurities on the spec-

tral density u of BID systems. The presence of impurities forces zeroes in $u(\omega)$,^{35,36} thereby constraining mode transitions. Moreover, as impurity concentration increases, the spectral density in the interval $[4K/m_I \leq \omega^2 \leq 4K/m_o]$ (assuming $m_I > m_o$) becomes increasingly suppressed, eventually containing isolated delta functions.^{37,38} If the frequency of the initial displacement is in the interval $[0 \leq \omega^2 \leq 4K/m_I]$, the mode will be in a continuous portion of $u(\omega)$ for all values of impurity concentration. As the impurity concentration increases, new modes will be generated more slowly, and in proximity to the original frequency.

VI. LENGTH AND TIME SCALES

At the lowest impurity concentrations, the chain is composed of long segments of homogeneous nonlinear chain. As new modes are generated, these modes are not localized and begin to propagate ballistically along the chain. The wave will continue to propagate until it scatters from an impurity or undergoes a spontaneous transition. A spontaneous transition along the homogeneous portion of the chain is unlikely to occur in the time required to span the distance between impurities. It is more likely that the impurities will initiate scattering and mode transitions. The mean free path $\Lambda = (c\sigma)^{-1}$ characterizes the effective transport coefficient $D(\omega)$:

$$D(\omega) = v_g \Lambda \quad (24)$$

Based on this assumption, thermal dissipation coefficient should be proportional to c^{-1} at the lowest concentrations.

As the impurity concentration increases, the localization length decreases and the wave experiences considerably more wave interference, and transport is more diffusive because any propagation is now limited by localization. The relevant time scale is the time t_ξ required for energy to diffuse a distance comparable to the localization length ξ :

$$D(\omega) = \frac{\xi^2}{t_\xi} \quad (25)$$

When this occurs, the thermal transport coefficient should become proportional to c^{-2} .

VII. RESULTS

The primary experimental parameter was impurity concentration c . The impurity concentration lower limit was constrained by computing resources. A previous study of these systems revealed that approximately 32 impurities are required in a chain to ensure reliable ensemble statistics.²³ The upper concentration limit was 0.5. Above this concentration, the behavior is indistinguishable from a complimentary study of the pure system having mass m_I and impurity mass m_o .

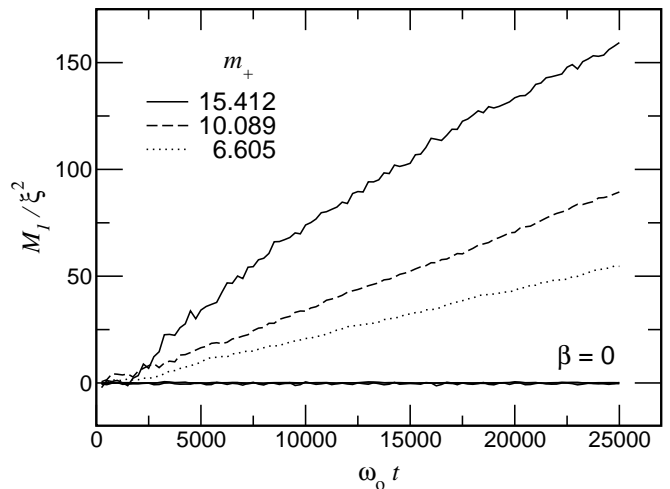


FIG. 10: The ratio M_1/ξ as a function of time for the systems having impurity concentration 0.500 and length 16 000. The $\beta = 1$ data have positive slopes and all the $\beta = 0$ data fall on top of one another.

Some of the results include estimates of uncertainty for quantities calculated from ensemble averages. For a calculation performed on an ensemble of W systems, there is a population standard deviation s and an average value. For this study, the average value is the meaningful quantity. The uncertainty in the reported average value is s/\sqrt{W} , and is referred to here as the standard deviation in the mean (SDM).

There are two special cases within the parameter space that require special consideration. The M_n data for the nonlinear systems are only meaningful when the M_n data for the corresponding harmonic system is a constant. This must be true for all cases, especially at concentrations for which $c\lambda \gg 1$.

In theory, M_n for harmonic systems would be a constant for all time. In practice, the mapping of the continuum system onto the discrete lattice, and the relocation of the ends, introduced a small amount of instability that led to small fluctuations in M_n . These fluctuations, however, were far smaller than the changes for the anharmonic systems.

As a brief example, Fig. 10 is a plot of M_1 as a function of time for systems having having impurity concentration 0.500 and length 16 000. In the figure, the $\beta = 1$ data appear as lines having positive slope. The harmonic $\beta = 0$ data for all three impurity masses lie upon one another near $M_1 = 0$. Figure 10 is doubly instructive. It demonstrates that the oscillations for the $\beta = 0$ data are negligible, even for the systems for which M_1 has the smallest values. Moreover, the harmonic data remain stable in concentrated systems: $c\lambda \gg 1$.

TABLE I: Interval from which δ_n was calculated for systems having length L .

L	Interval
16000	$5000 < \omega_o t < 20000$
32000	$10000 < \omega_o t < 25000$
64000	$20000 < \omega_o t < 50000$
96000	$20000 < \omega_o t < 80000$

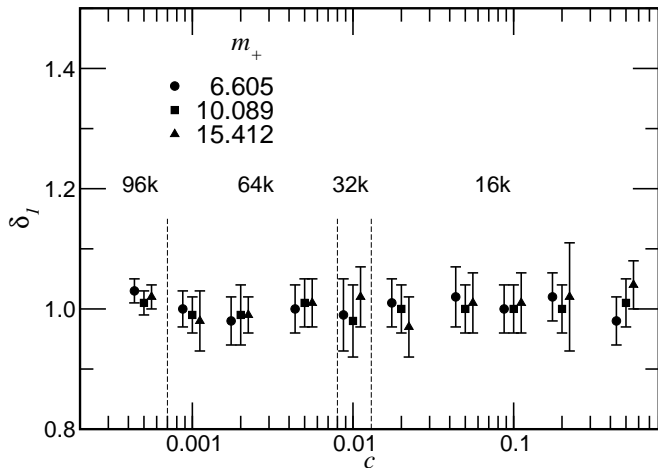


FIG. 11: The time exponent δ_1 for G_1 as a function of impurity concentration c for impurity cross sections $\sigma = 0.30, 0.50, 0.70$. Numbers between vertical dashed lines denote N ($k=1000$).

A. Time Exponent

A quantitative characterization of M_n is made by assuming a power-law dependence on time t :

$$M_n = 2G_n t^{\delta_n} \quad (26)$$

The first task is to determine the value of the exponent so as to distinguish among ballistic, diffusive, or subdiffusive transport. The calculation of δ_n is affected by initial transients, and the details of the analysis are given in the Appendix. The time interval from which the values of δ_n were calculated were constrained by the initial transients at small times and total energy conservation at long times. The specific intervals are shown in Table I for each system length.

The results of the analyses for δ_1 are summarized in Fig. 11 for all the systems. (In the figure, the symbols at a particular concentration are displaced horizontally to distinguish individual error bars representing the SDM.) With only one exception, the estimated values for δ_1 are within one SDM of 1. Therefore, subsequent analysis of M_1 is based on linear model with respect to time.

Results of the analysis for δ_2 are shown in Fig. 12 for the same systems. Although the values of δ_2 are near 1 for most systems, there is considerably more variability

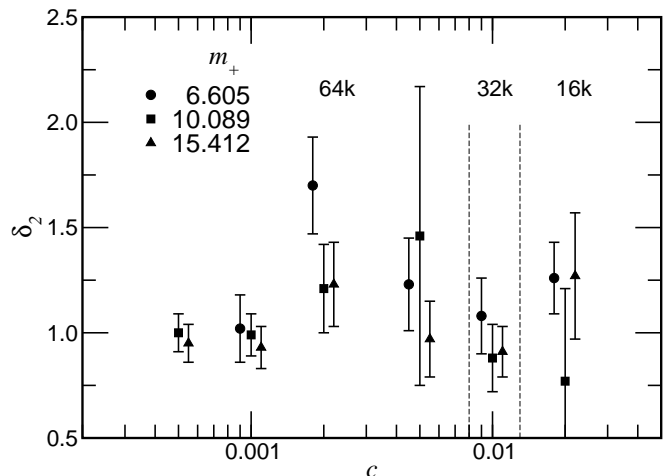


FIG. 12: The time exponent δ_2 for G_2 as a function of impurity concentration c for impurity cross sections $\sigma = 0.30, 0.50, 0.70$. Numbers between vertical dashed lines denote system size used ($k=1000$).

than for δ_1 . Moreover, it was difficult to establish a precise value for δ_2 at higher concentrations. As a result, subsequent analysis is confined to M_1 .

According to Li et al.,³⁹ if the mean squared displacement of a particle is proportional to t^α with ($0 \leq \alpha \leq 2$), the thermal conductivity can be expressed as a function of the system size L : $\kappa \sim L^b$ with $b = 2 - 2/\alpha$. Therefore, a system obeying normal diffusion implies normal heat conduction obeying Fourier's law ($b = 0$).

B. Transport Coefficient

Because δ_1 was shown to be within one SDM of 1, the determination of $2G_1$ is based on the assumption of a linear relationship between M_1 and t over the same intervals shown in Table I. Although M_1 was determined by linear regression with a linear model, calculating the uncertainty in M_1 required a slightly more involved analysis; details are given in the Appendix.

Estimates of $2G_1$ for all the systems considered are plotted in Fig. 13 as a function of the impurity concentration c . The calculated values appear as filled symbols having error bars that represent the SDM. The thin solid lines connecting the symbols are only to guide the eye. The two dashed line segments appearing above the data indicate slopes that are proportional to $1/c$ and $1/c^2$. The three dotted lines are proportional to ξ , as they appear in Fig. 3.

From the data in Fig. 13, there appear to be three regions of interest. At low concentration, the transport coefficient G_1 is proportional to c^{-1} , as was expected from the discussion of time and length scales. As the impurity concentration increased, and the diffusion time t_ξ decreases sufficiently that Eq. (25) dominates, and G_1 becomes proportional to c^{-2} . This transition is not ap-

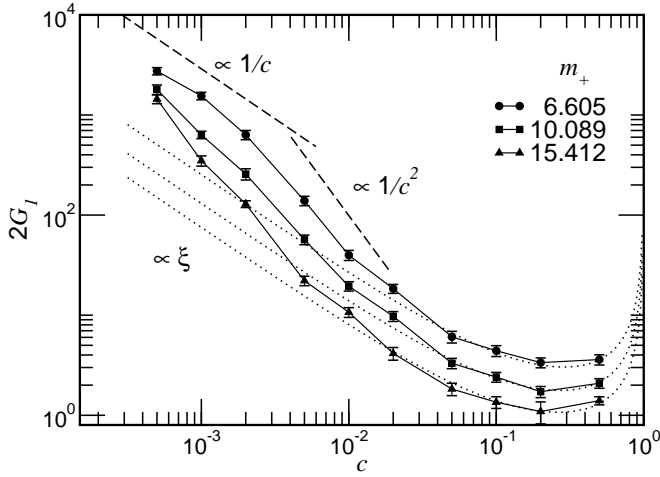


FIG. 13: Transport coefficient G as a function of impurity concentration c for impurity cross sections $\sigma = 0.30, 0.50, 0.70$. Dashed line is proportional to c^{-1} . Dotted line is proportional to ξ .

parent in the results of Payton *et al.*²⁷ on a similar system having thermostats because their computing resources prevented them from resolving the smaller concentrations required to see the effect.

There is a noticeable difference in the rate at which the three curves make the transition from c^{-1} to c^{-2} . Based on the transition data for similar FPU- β systems, the transition rate should be inversely proportional to the impurity mass m_I .³¹ Therefore, the transition rate for the $m_+ = 15.412$ is slowing more rapidly, for a given change in impurity concentration, than the other two impurity masses. As a result, the $m_+ = 15.412$ systems do not exhibit distinct $1/c$ dependence at the concentrations studied.

The interesting behavior was the final transition at higher concentrations to a transport coefficient that is proportional to the initial localization length ξ . The three dotted curves labelled $\propto \xi$ are proportional to the localization lengths that appear in Fig. 3 for $\lambda = 31.8$. The value of ξ is multiplied by the same coefficient (approximately 0.09) to make the curves best agree with the measured transport coefficient.

C. Localization Parameter

The localization parameter can also be used as a measure of energy propagation. Although systems of different lengths were used, energy transport, starting from a localized state, should be independent of total system length. Based on the previous discussion of the localization parameter, the ratio L/Γ is proportional to the number of masses over which the total energy is distributed. For a given m_I and c , and assuming that $L \gg \xi$, the number of masses, and not the fraction of the system (Γ_∞/Γ), should also be independent of total system length. There-

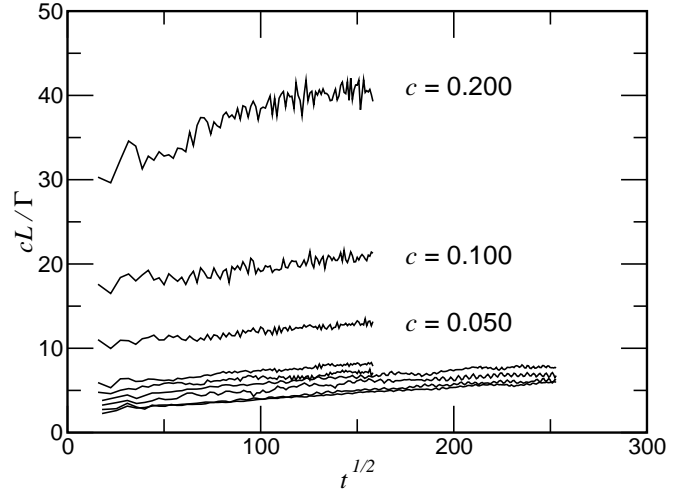


FIG. 14: Localization parameter Γ as a function of time $t^{1/2}$ for systems having $m_+ = 6.605$.

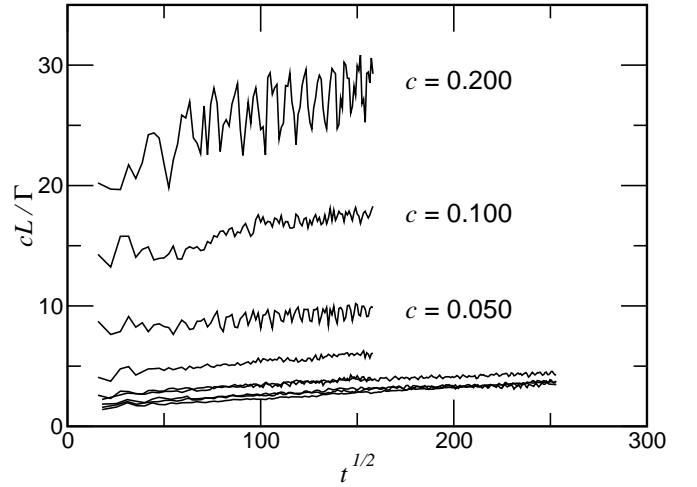


FIG. 15: Localization parameter Γ as a function of time $t^{1/2}$ for systems having $m_+ = 10.089$.

fore, the ratio L/Γ will serve as a means for comparing results from systems of different lengths.

If the linear time dependence of the second moment M_1 indicates diffusive behavior, the number of masses involved in energy transport should increase in proportion to $t^{1/2}$. In addition, because transport in dilute systems is proportional to c^{-1} , the quantity $cL\Gamma$ should approach a constant for systems with low impurity concentrations. The quantity cL/Γ , as a function of $t^{1/2}$, is plotted in Figs. 14–16 for most of the systems studied. In the figures, curves for smaller impurity concentration appear consecutively lower in the graph.

There are two noteworthy features in Figs. 14–16. The number of masses participating appears to be linear over the time intervals considered, particularly for the dilute impurity systems. This is consistent with the expectation of diffusive energy transport. Also, as expected, the curves for the most dilute impurity concentrations appear

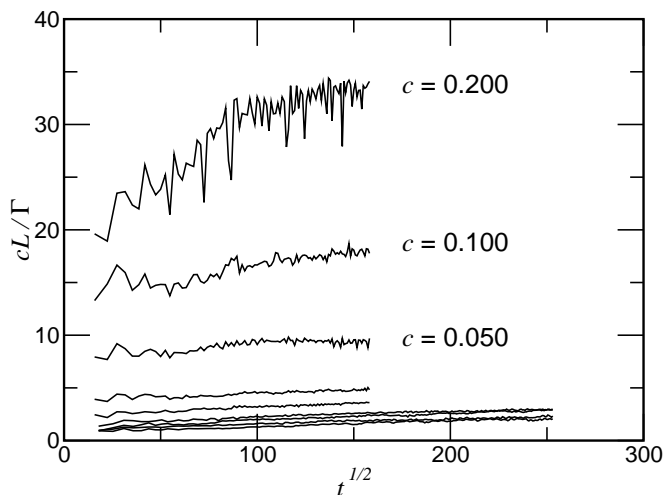


FIG. 16: Localization parameter Γ as a function of time $t^{1/2}$ for systems having $m_+ = 15.412$.

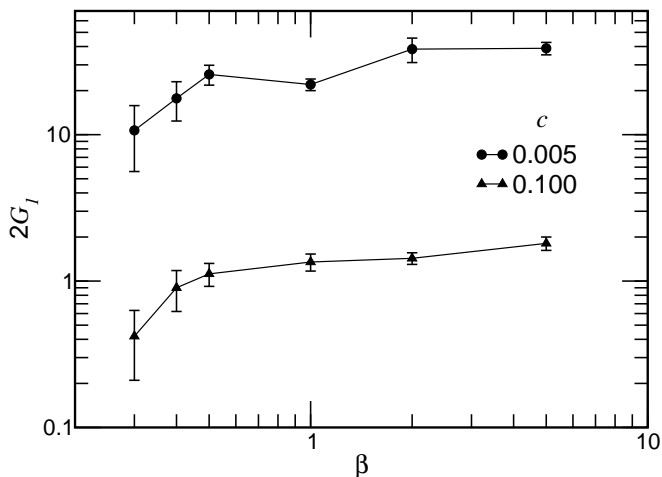


FIG. 17: Transport coefficient G as a function of β for two impurity concentrations: $c = 0.100, 0.005$, and $\sigma = 0.70$.

to approach an asymptote, supporting the c^{-1} dependence for the number of masses participating in energy transport.

VIII. DISCUSSION

A. β -Dependence

It was argued that the results given for $\beta=1$ are indicative of results for ‘large’ values of β that are above the critical threshold that leads to ergodic behavior. As a check, the value of G_1 for two systems are calculated for different values of β . The two systems are ($c = 0.005, \sigma = 0.70$) and ($c = 0.100, \sigma = 0.70$). The analysis for these systems was carried out in a manner identical to that for the $\beta = 1$ data.

The values for G_1 are shown in Fig. 17 as a function

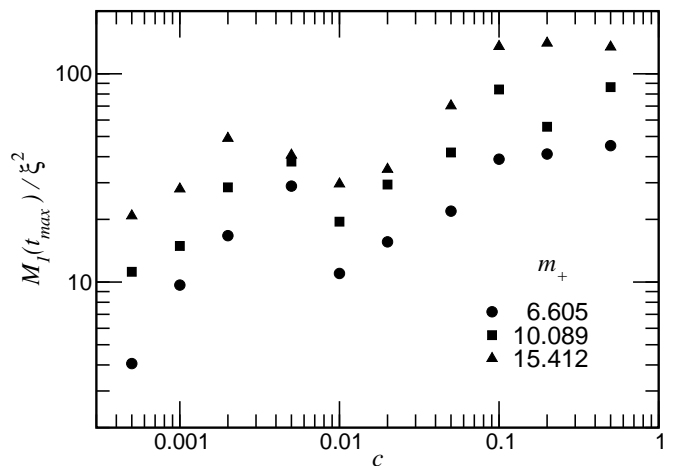


FIG. 18: The ratio $M_1(t_{max})/\xi^2$ as a function of impurity concentration c .

of β . Over the time interval studied, values of G_1 decreased for values of β below 0.5, falling to near zero at $\beta = 0.2$. For $0.5 \leq \beta \leq 5.0$, the transport coefficient has a weak dependence on the anharmonicity, which is consistent with numerical experiments on finite temperature nonlinear BID systems.²⁷ Therefore, while the calculated values of G are not constant, there does not appear to be any significance to a particular value for β that is greater than 0.5.

B. Diffusion Time t_ξ

The coefficient $2G_1$ in Fig. 13 represents the transport coefficient that characterizes the time t_ξ , defined in Eq. (25):

$$t_\xi \approx \xi^2/G_1 \quad (27)$$

At low concentration, because both G_1 and ξ are proportional to c^{-1} , the diffusion time t_ξ must also be proportional to c^{-1} . At intermediate concentration, G_1 is proportional to c^{-2} , so t_ξ is a weak function of impurity concentration. At the highest concentrations studied, G_1 and t_ξ are both proportional to ξ . At these concentrations, however, ξ is a weak function of impurity concentration, so the same must be true for t_ξ .

C. Time Scale

The significance of the reported results presented depends, in part, on the relative duration of the calculation. One measure of duration, to gauge whether long times have been probed, is the ratio of the distance energy propagates along the system to its initial span. The maximum energy propagation length is proportional to $M_1(t_{max})$, and the initial span is proportional to the initial localization length ξ .

The ratio $M_1(t_{max})/\xi^2$ for each system is plotted in Fig. 18. The ratio varied from 10 to 100, increasing with impurity concentration. The square root of this ratio is a measure of the depth to which energy propagated to the initial depth energy was distributed. Therefore, energy penetration depth, relative the initial localization length, varied from 3 to 10.

Extending this experiment to longer times will probably yield similar results. It is unlikely that ballistic transport will occur at long times. As the calculation progresses, the energy is being distributed over a greater number of masses. Because both energy and transition rates are proportional to the square of the oscillation amplitude, the mode transition rate is decreasing in proportion to $t^{-1/2}$.

D. Memory Effect

Although previous arguments address why the transport coefficient should vary from c^{-1} to c^{-2} , they do not explain why the transport coefficient should be proportional to ξ at the highest concentrations. More specifically, it was unexpected that the transport coefficient is proportional to the original localization length and not some averaged value. Figure 18 shows that the energy has propagated nearly ten times the localization length for the highest impurity concentrations, yet these systems seem to retain some “memory” of the initial state.

An explanation may be made from the results of the hoop experiment shown in Fig. 9. For those systems, both the number of modes and the transition rate decreased significantly with increasing impurity concentration. At these concentrations and time scales, mode generation may have been dominated by impurity scattering. As the localization length is quite small for most modes, any new mode could only propagate a short distance before becoming localized. If the impurities constrained mode generation sufficiently so that generated modes had frequencies near the initial mode, the initial localization length would remain as the controlling length scale over which new modes could propagate before scattering again.

IX. CONCLUSION

For systems initially localized near one end of a FPU- β chain, anharmonicity facilitates energy transport along the chain. For energy eigenstates of harmonic disordered chains, sufficient anharmonicity leads to diffusive energy transport. The second moment of the site energies was linear over times long enough for energy to have propagated a distance nearly equal to ten times the initial spatial extent of the pulse. Although direct mass displacement observation showed low frequency modes propagating ballistically, the energy content in these modes was insufficient for super-diffusive energy transport.

Alternate measures of energy and frequency distribution corroborated the assertion of diffusive behavior. We found that the localization parameter was proportional to the square root of time, suggesting that energy distributes itself among masses in a diffusive manner. This diffusive short range behavior is consistent with the observation of more long range diffusive behavior. Calculations of the relative number of modes participating in periodic (hoop) systems suggest that an increase in the number of impurities reduces the number of active modes.

The most interesting aspect of the transport coefficient was the concentration dependence. At the lowest impurity concentration c values, the transport coefficient was proportional to c^{-1} . At higher impurity concentrations, the transport coefficient developed a c^{-2} dependence. These two concentration dependences are consistent with arguments based on the competition between diffusion times and mode transition rates.

At the highest impurity concentrations, the transport coefficient was proportional to the original localization length. The postulated cause for this was from the severe suppression of new frequency modes that occurs in concentrated BID systems. These new modes, having a frequency in proximity of the original frequency, experienced a similar localization length, which dominated the distance travelled before subsequent scattering events. As a result, the original localization length remained the dominant length scale over which transport occurred for any given phonon.

Acknowledgments

The authors would like to thank Dr. Jack Douglas of the Polymers Division (NIST) for his useful comments and discussion. This work was supported by the NSF under grant number DMR-01-32726, and by the National Institute of Standards and Technology (NIST) High Performance Construction Materials and Systems program in the Building and Fire Research Laboratory.

APPENDIX: DATA ANALYSIS

The analyses of the results involve some minor subtleties that deserve a clear exposition. Neglecting these subtleties and performing an ordinary least squares (OLS) analysis of the data would lead to misleading results. Specifically, not adjusting for initial transient behavior would lead to a different conclusion regarding the existence of diffusive energy transport.

As mentioned previously, the reported uncertainties are the standard deviation in the mean (SDM) calculated from the ensemble population standard deviation s . For an ensemble of W systems, the SDM reported here is s/\sqrt{W} . This uncertainty characterizes the reported average value from the population.

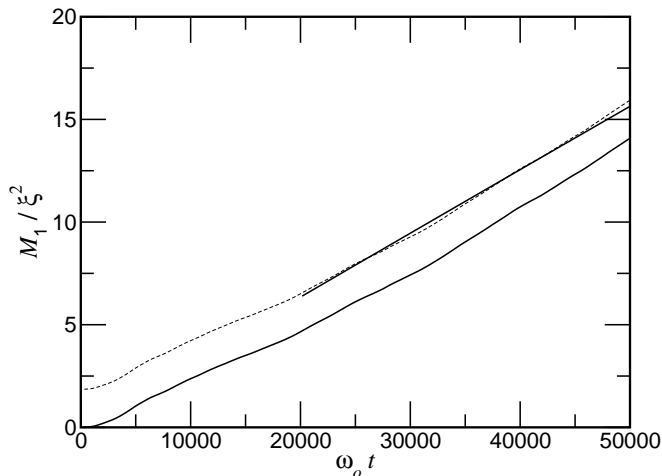


FIG. 19: M_1/ξ^2 as a function of time. System length is 64 000, impurity concentration is 0.002, single impurity cross section is 0.30. The measured data appear as a solid line, the shifted data appear as dashed line, and the line segment denotes the range over which regression was performed.

1. Energy Fluctuation

For each calculation, the total energy $\Upsilon(t)$ was calculated as a function of time. Due to randomness, the initial total energy fluctuates among the ensembles. To ensure that values of Υ were on comparable scales, the values were divided by the initial value $\Upsilon(0)$. The ratio $\Upsilon_m(t)/\Upsilon_m(0)$ ($1 \leq m \leq W$) is calculated as a function of time for each of the W systems composing the ensemble. The averaged values are calculated at each of the P values of t_i :

$$\bar{\Upsilon}(t_i) = \frac{1}{W} \sum_m^W \frac{\Upsilon_m(t_i)}{\Upsilon_m(0)} \quad 1 \leq i \leq P \quad (\text{A.1})$$

These averaged values, along with the population standard deviation, are pooled and stored in the output data file. The population of W values at t_i do not, unfortunately, represent energy fluctuation for a single system. Rather, it characterizes statistical fluctuations among the different systems, evaluated at the same time.

Energy fluctuation can only be approximated from fluctuations in the P average values of $\bar{\Upsilon}(t_i)$. The standard deviation $s_{\bar{\Upsilon}}$ of each $\bar{\Upsilon}(t_i)$ represents a standard deviation in the mean. The population standard deviation is approximated by $s_{\bar{\Upsilon}}\sqrt{P}$. This population standard deviation was never more than 0.2 %. Spot checks of $\Upsilon(t)$ in individual systems rarely gave a standard deviation greater than 0.2 %.

2. δ_n Analysis

The straightforward means of determining the time exponent δ_n is from the slope of a log-log plot of M_n versus

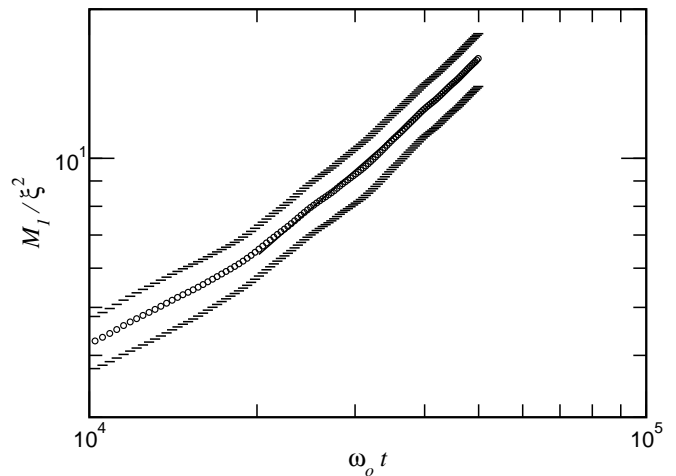


FIG. 20: A log-log plot of data in Fig. 19, along with horizontal error bars denoting the population standard deviation; the vertical risers are omitted for clarity. The solid line was determined by OLS regression applied to the mean values.

time t . This approach assumes that the power law dependence exhibits itself at $t = 0$. In reality, there is a transient period, after which the value of M_n begins to increase. Although this increase appears to be linear, the data must be corrected to eliminate the effect of the transient.

The effect of the transient behavior is negated by shifting the data for M_n vertically. OLS linear regression is applied to the M_n versus t data over the time intervals given in Table I. The intercept calculated from the OLS regression is subtracted from $M_n(t)$. The process is demonstrated in Fig. 19 for one particular system. The original M_1 data are shown as a solid line. Regression is applied to the interval [20000, 50000], and the data are shifted vertically so that the linear approximation to this interval has zero intercept.

OLS linear regression is then applied to the logarithm of these adjusted data versus the logarithm of time. The slope of this regression calculation is the value reported in Figs. 11 and 12 for δ_1 and δ_2 , respectively.

The uncertainty in δ_n is calculated from both the regression residuals and the ensemble population of M_n values. Fortunately, because the population standard deviation in M_n increases in time, the logarithm transform yields uncertainties that are nearly constant over the time intervals of interest. The adjusted data from Fig. 19 are shown in Fig. 20, along with the ensemble population standard deviations that are denoted by horizontal error bars; the vertical risers are omitted for clarity. (The ensemble population standard deviation, instead of the SDM, is shown in the figure for clarity of the demonstration. For an ensemble of W systems, the SDM error bars would be a factor of \sqrt{W} smaller than those shown in the figure.) Also shown in the figure is the result of the regression analysis of the average values. The error bars denote the ensemble uncertainty, and the residuals

represent the regression uncertainty.

The OLS linear regression in log-space will yield an estimated uncertainty (standard deviation) for slope that is a function of the standard error of the residuals. The standard error s can be used to estimate the regression standard deviation s_{reg} for the slope δ_n :

$$s_{reg} = \frac{s}{\sqrt{S_{XX}}} \quad (\text{A.2})$$

where the quantity S_{XX} is the sum of squares:

$$S_{XX} = \sum_i (\ln t_i - \overline{\ln t})^2 \quad (\text{A.3})$$

The quantity $\overline{\ln t}$ represents the average value over the specified interval.

The uncertainty in δ_n should also reflect the SDM recorded for the ensemble s_{ens} . It is assumed that these two uncertainties are independent of one another, and that they are additive. The uncertainty (estimated standard deviation) in the time exponent is

$$s_{\delta_n}^2 = \frac{s_{res}^2}{S_{XX}} + \frac{s_{ens}^2}{S_{XX}} \quad (\text{A.4})$$

Because s_{ens} is the majority of s_{δ_n} , the uncertainty in δ_n is referred to as a SDM, and the coverage factor is approximately equivalent to one standard deviation for a normal distribution.

3. M_1 Analysis

Based on the results of the δ_1 analysis, a hypothesis of a linear relationship between the second moment M_1 and time t cannot be rejected. The ability to use a linear model simplifies the analysis of M_1 . The transport coefficient $2G_1$ is the slope that is calculated from OLS regression using a linear model.

The uncertainty in $2G_1$ cannot be determined from a regression analysis of the M_1 versus t data because the uncertainties in M_1 increase in time. Fortunately, the data can be transformed into a more suitable format.

Assuming diffusive behavior, the values of M_1 are a collection of lines, radiating from the origin. The error model for the observations assumes that there exists an inherent error ϵ and that the total error increases with time:

$$M_n(t_i) = A + 2G_n t_i + t_i \epsilon_i \quad (\text{A.5})$$

To use OLS techniques, the error term must be additive and constant. Equation (A.5) can be transformed into a suitable model:

$$\frac{M_n(t_i)}{t_i} = \frac{A}{t_i} + 2G_n + \epsilon_i \quad (\text{A.6})$$

Unfortunately, the initial transient behavior that confounded the calculation of δ_n must also be accounted

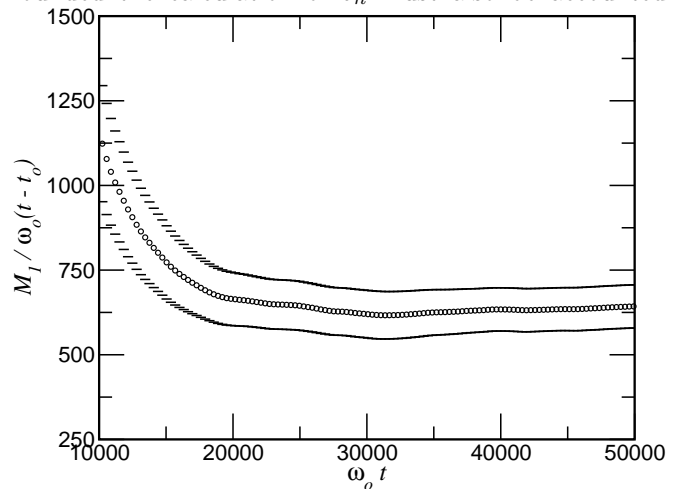


FIG. 21: Transformed M_1 to demonstrate how uncertainty in δ_1 is calculated.

for here. The error model assumes that the uncertainty grows linearly from $t = 0$. In reality, the increase in M_n occurred after some initial transient time t_o . To correct for this, linear regression is applied to the M_1 versus t data to determine the value of t_o . Using t_o , the data are shifted horizontally so that the linear region of interest points to the origin. These shifted data are then transformed according to Eq. (A.6).

The result of this transform, applied to both the mean and SDM, is shown in Fig. 21 for the data in Figs. 19 and 20. In Fig. 21, the error bars represent the SDM. Over the range of regression (see Table I), the SDM is relatively constant, consistent with Eq. (A.6). Because the model in Eqn. (A.6) assumes a constant factor of $2G_1$, the error bars in Fig. 21 represent the SDM for $2G_1$.

¹ T. Held, I. Pfeiffer, and W. Kuhn, Phys. Rev. B **55**, 231 (1997).

² S. Rohmfeld, M. Hundhausen, L. Ley, N. Schulze, and G. Pensl, Phys. Rev. Lett. **86**, 826 (2001).

³ F. Widulle, J. Serrano, and M. Cardona, Phys. Rev. B **65**,

075206 (2002).

⁴ M. Wagner, G. Zavt, J. Vazquez-Marquez, A. Lütze, T. Mougios, G. Viliani, W. Frizzera, O. Pilla, and M. Montagna, Philos. Mag. B **65**, 273 (1992).

⁵ I. Y. Solodov and B. A. Korshak, Phys. Rev. Lett. **88**,

- 014303 (2002).
- ⁶ I. Solodov, J. Wackerl, K. Pfeiderer, and G. Busse, *Appl. Phys. Lett.* **84**, 5386 (2004).
 - ⁷ P. W. Anderson, *Phys. Rev.* **109**, 1492 (1958).
 - ⁸ R. Bourbonnais and R. Maynard, *Phys. Rev. Lett.* **64**, 1397 (1990).
 - ⁹ R. Bourbonnais and R. Maynard, *Int. J. Mod. Phys. C* **1**, 233 (1990).
 - ¹⁰ A. Sarmiento, R. Reigada, A. H. Romero, and K. Lindenberg, *Phys. Rev. E* **60**, 5317 (1999).
 - ¹¹ H. Yamada and K. S. Ikeda, *Phys. Rev. E* **59**, 5214 (1999).
 - ¹² A. Rosas and K. Lindenberg, *Phys. Rev. E* **69** (2004).
 - ¹³ E. Fermi, J. Pasta, and S. Ulam, Tech. Rep. LA-1940, Los Alamos Scientific Laboratory (1955), See also: *The Many-Body Problem*, edited by D.C. Mattis, World Scientific, 851–870, (1993).
 - ¹⁴ E. Helfand, *Phys. Rev.* **119**, 1 (1960).
 - ¹⁵ T. Cretegny, T. Dauxois, S. Ruffo, and A. Torcini, *Physica D* **121**, 106 (1998), cond-mat/9709204.
 - ¹⁶ F. Piazza, S. Lepri, and R. Livi, *J. Phys. A* **34**, 9803 (2001).
 - ¹⁷ H. Yoshida, *Phys. Lett. A* **150**, 262 (1990).
 - ¹⁸ R. Livi, M. Pettini, S. Ruffo, M. Sparpaglione, and A. Vulpiani, *Phys. Rev. A* **31**, 1039 (1985).
 - ¹⁹ R. Khomeriki, S. Lepri, and S. Ruffo (2004), cond-mat/0407134.
 - ²⁰ R. de L. Kronig and W. G. Penney, *Proc. Roy. Soc. Lond. A* **130**, 499 (1931).
 - ²¹ J. M. Ziman, *Models of Disorder* (Cambridge University Press, Cambridge, 1979).
 - ²² P. M. Morse and K. U. Ingard, *Theoretical Acoustics* (Princeton University Press, 1968).
 - ²³ K. A. Snyder and T. R. Kirkpatrick, *Phys. Rev. B* **70**, 104201 (2004).
 - ²⁴ C. Kittel, *Introduction to Solid State Physics* (Wiley, 1986), sixth ed.
 - ²⁵ P. W. Anderson, D. J. Thouless, E. Abrahams, and D. S. Fisher, *Phys. Rev. B* **22**, 3519 (1980).
 - ²⁶ R. Landauer, *Philos. Mag.* **21**, 863 (1970).
 - ²⁷ D. N. Payton, M. Rich, and W. M. Visscher, *Phys. Rev.* **160**, 706 (1967).
 - ²⁸ D. J. Evans and G. P. Morriss, *Statistical Mechanics of Nonequilibrium Liquids* (Academic Press, London, 1990).
 - ²⁹ D. J. Evans, *Phys. Lett.* **91A**, 457 (1982).
 - ³⁰ J. Fröhlich, T. Spencer, and C. E. Wayne, *J. Stat. Phys.* **42**, 247 (1986).
 - ³¹ K. A. Snyder and T. R. Kirkpatrick, *Ann. Phys. (Leipzig)* **8**, SI 241 (1999).
 - ³² T. Cretegny, T. Dauxois, S. Ruffo, and A. Torcini, *Localization and equipartition of energy in the beta-FPU chain : Chaotic breathers* (1997), cond-mat/9709204.
 - ³³ L. Brillouin, *Science and Information Theory* (Academic Press, New York, 1956).
 - ³⁴ J. D. Luca and A. Lichtenberg, *Phys. Rev. E* **66**, 026206 (2002).
 - ³⁵ D. S. Saxon and R. A. Hunter, *Philips Res. Rep.* **4**, 81 (1949).
 - ³⁶ J. M. Luttinger, *Philips Res. Rep.* **6**, 303 (1951).
 - ³⁷ J. Hori, *Spectral Properties of Disordered Chains and Lattices* (Pergamon Press, Oxford, 1968).
 - ³⁸ D. N. Payton and W. M. Visscher, *Phys. Rev.* **175**, 1201 (1968).
 - ³⁹ B. Li and J. Wang, *Phys. Rev. Lett.* **91**, 044301 (2003).